Biophysical Chemistry 173–174 (2013) 1–7

Contents lists available at SciVerse ScienceDirect

Biophysical Chemistry

journal homepage: http://www.elsevier.com/locate/biophyschem

A T_3R_3 hexamer of the human insulin variant B28Asp

Leonardo C. Palmieri [a], Maely P. Fávero-Retto [a,b,c], Daniela Lourenço [d], Luís Mauricio T.R. Lima [a,d,e,*]

[a] School of Pharmacy, Federal University of Rio de Janeiro — UFRJ. CCS, Bss34, Ilha do Fundão, 21941-590, Rio de Janeiro, RJ, Brazil
[b] Brazilian National Cancer Institute (INCA), 20230-014, Rio de Janeiro, RJ, Brazil
[c] Brazilian National Institute of Traumatology and Orthopedics (INTO), Rio de Janeiro, RJ, Brazil
[d] Laboratory for Biotechnology (LaBio-DIPRO), Brazilian National Institute of Metrology, Quality and Technology — INMETRO, Rio de Janeiro, Brazil
[e] National Institute of Science and Technology for Structural Biology and Bioimaging (INBEB-INCT), Federal University of Rio de Janeiro, Rio de Janeiro 21941-590, Brazil

HIGHLIGHTS

- The aspart insulin variant is a fast-acting due to improved monomerization.
- We have crystallized the aspart insulin in the T_3R_3 conformation.
- Hexamer stability is supported by B3Asn interaction.
- Existence of monomers, dimers and hexamer is supported by SAXS, ion-mobility spectrometry and crystallography.

GRAPHICAL ABSTRACT

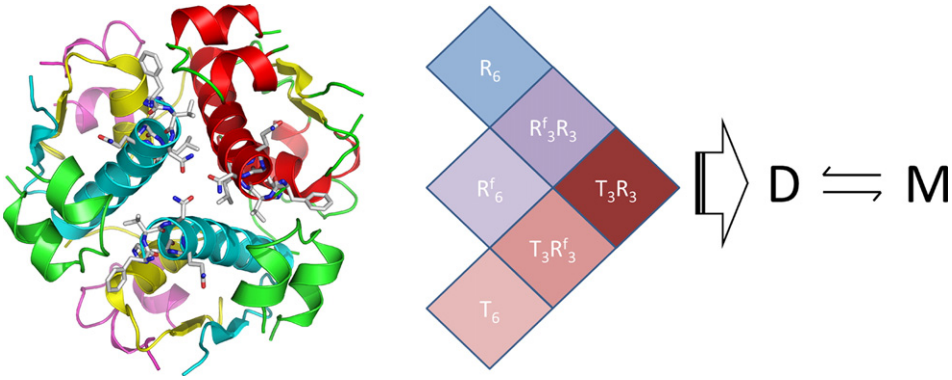

ARTICLE INFO

Article history:
Received 1 December 2012
Received in revised form 1 January 2013
Accepted 4 January 2013
Available online 4 February 2013

Keywords:
Human insulin
Crystallography
Nuclear magnetic resonance
Mass spectroscopy
Small-angle X-ray scattering

ABSTRACT

Insulin shows a complex equilibrium between monomers and hexamers, involving varying conformers and association states. We sought to perform a structural characterization of the fast-acting human insulin variant B28Asp ("aspart"). Small-angle X-ray scattering measurements reveal similar globular behavior in both the aspart and regular human insulin, with a R_g of 19 Å and a D_{max} of approximately 50 Å, indicating similar mean quaternary assembly distribution. Crystallographic assays revealed a T_3R_3 assembly of the aspart insulin formed by the TR dimer in the asymmetric unit, with all the first 8 residues of the B chain in the R-state monomer in helical conformation and the participation of its B3Asn in the stabilization of the hexamer. Our data provide access to novel structural information on aspart insulin such as an aspart insulin dimer in solution, the aspart insulin in T conformation and a pure R-state conformer establishing a T_3R_3 assembly, providing further insight on the stepwise conformational transition and assembly of this fast-insulin.

1. Introduction

Insulin is a pancreatic hormone that regulates glucose homeostasis. The mature insulin molecule comprises two polypeptide chains A and B, linked by disulfide bonds. High-resolution and high-definition spectroscopic techniques, such as crystallography, nuclear magnetic resonance (NMR) and ion mobility spectroscopy (IMS), have long been used in the structural characterization of insulin [1–8].

Abbreviations: SAXS, small-angle X-ray scattering; ESI–IMS–MS, electron-spray ionization–ion mobility spectrometry–mass spectrometry; MALDI, matrix-assisted laser desorption and ionization; TOF, time of flight; HDMS, high definition mass spectrometry.

* Corresponding author at: School of Pharmacy, Federal University of Rio de Janeiro — UFRJ. CCS, Bss34, Ilha do Fundão, 21941-590, Rio de Janeiro, RJ, Brazil. Tel./fax: +55 21 2562 6639.
E-mail address: LML@UFRJ.BR (L.M.T.R. Lima).

0301-4622/$ – see front matter © 2013 Elsevier B.V. All rights reserved.
http://dx.doi.org/10.1016/j.bpc.2013.01.003

Insulin has been shown to assembly in the T and R conformation, in which the aminoacids B1 to B8 vary from an extended to an α-helical conformation respectively. Insulin has been reported to assembly into hexamers in the T_6 (e.g., PDB ID 1MSO), $T_3R_3^f$ (e.g. PDB ID 1TRZ from single crystal, PDB entry 1FUB and 1FU2 from powder diffraction), T_3R_3 (e.g. PDB ID 2QIU), and R_6 (e.g., PDB ID 1EV6) conformers, where T states for "tense" conformer, R for "relaxed" and R^f states for "frayed," in which the amino acids B1–B3 are in extended conformation and B4–B8 are in helical conformation equivalent to the R-conformation [9–11].

Mutational analysis of human insulin has shown that some point mutant can result in weakening of the hexameric form, resulting in increased propensity for dissociation into the active monomeric form and thus a quicker delivery of insulin [12], including the human insulin analog B28 Pro→Asp (aspart insulin), a therapeutic form of insulin for fast-acting, meal-time administration [12–16]. To date, the crystal structure of the aspart insulin has only been reported in a R_6 assembly [13] and there is a lack for evidences of intermediate oligomeric species between hexamers and monomers. We sought to perform a structural characterization of the aspart insulin from the pharmaceutical formulation, since ultimately it would provide a deeper insight on their structure–function relationship [17]. In the present work we report the T_3R_3 hexamer of the aspart insulin, in which the R-monomer is shown with the whole segment comprising the first 8 residues of the B chain N-termini in α-helical conformation. Along with additional high-resolution spectroscopic data by ion mobility mass spectrometry and small-angle X-ray scattering (SAXS) characterizing the oligomeric distribution and conformation of the aspart insulin in solution, we discuss our findings in light of the weakening of monomer–monomer interaction which would favor the enhanced propensity for hexamer dissociation of the aspart human insulin variant.

2. Materials and methods

2.1. Chemicals

Human insulin formulations at 100 U/mL were acquired direct from drug store and kept under refrigeration at 4 °C until use. In this work, we used the human insulin analog B28 Pro→Asp (Aspart insulin, NovoRapid Penfill Aspart Insulin, Novo Nordisk, Brazil, lot # XS62590) and wild-type, regular human insulin (Novolin® R; Novo Nordisk, Brazil, lot # TS62953). According to the manufacture's product leaflet, the composition of the aspart formulation is the following: insulin aspart (rDNA origin) 100 U/mL, glycerol, phenol, metacresol, zinc, disodium hydrogen phosphate dihydrate, sodium chloride and water for injection, pH of 7.2–7.6. According to the manufacture's product leaflet, the composition of the regular human insulin is the following: human insulin (rDNA origin) 100 U/mL, glycerol, metacresol, zinc chloride and water for injection, pH of 7.4. D_2O 99.8% was purchased from Sigma-Aldrich (Saint Louis, USA). All other reagents were of analytical grade.

2.2. Electron-spray ionization–ion mobility spectrometry–mass spectrometry (ESI–IMS–MS) measurements

ESI–IMS–MS measurements were performed in a MALDI-Synapt G1 (Waters Brazil) high definition mass spectrometer (HDMS) quadrupole-traveling wave mass spectrometer. Protein samples were diluted 20 times from their original concentration in the finished pharmaceutical formulation using either i) 100 mM ammonium acetate buffered to pH 7.4 using ammonium hydroxide (for native measurements) or ii) 49% methanol in water containing 1% formic acid (for measurements at denaturing conditions). Samples were injected at a rate of 100 nL/min, using a positive ESI with a capillary voltage of 2.8 kV and N_2g at 0.4 bar. Data were acquired over the range of m/z 500 to 2,200 for 5 min per acquisition with repeated 3 s acquisition time per point. Mass calibration was performed on a dynamic mode. Other typical experimental settings involved sampling and extraction cone set respectively at 30 V/5.0 V, source temperature of 70 °C, and nanoflow gas pressure of 400 mbar. The trap (before IM cell) and transfer (after IM cell) cells voltage were set to 6 and 4 V, respectively. The cell pressures were controlled by argon gas, while IM separations were performed by using N_2g, and transfer wave velocity of 248 m/s and transfer wave amplitude set at 3.0 V. Data were analyzed using DriftScope 2.1 [18] (Waters Corporation, Brazil) and MassLynx 4.1 (Waters Corporation, Brazil).

2.3. Small angle X-ray scattering

SAXS experiments were carried out using the D11-SAS1 beam line [19] on the LNLS. SAXS data were collected directly from insulin formulations using a two-dimensional detector (MarCCD; MarResearch, USA) at wavelength of 1.488 Å with the sample-detector distance providing a q-range from 0.02 $Å^{-1}$ to 0.25 $Å^{-1}$, where q is the modulus of the scattering vector (calculated according to $q=(4\pi/\lambda)\sin\theta$, where λ is the wavelength used and 2θ is the scattering angle). The scattering curves of the protein solutions and buffers were collected in several successive frames of 500 s each to monitor for radiation-induced protein oxidation. The data reduction routine included normalization of the one-dimensional scattered data to the intensity of the transmitted incident beam; correction for detector response, incident beam intensity and sample absorption; and blank subtraction using scattering from water.

A Guinier analysis of solution scattering [20] was applied to evaluate the presence of aggregates and to determine the apparent radius of gyration (R_g) of insulin in solution [14,21,22]. The R_g and the scattered intensity, $I(q)$, were inferred, respectively, from the slope and the intercept of the linear fit of $\ln[I(q)]$ versus q^2 in the q-range $q^*R_g<1.3$ [20]. The same parameters were also obtained from the data fit of the merged curve by the indirect Fourier transform program Gnom [23], which also evaluated the distance-distribution function, $P(r)$, of insulin. The maximum dimension, D_{max}, was estimated from the distance distribution function $P(r)$, with limiting distance r where $P(r)$ first converges down to zero.

The SAXS data were analyzed by fitting the theoretical scattering intensities computed from the models of monomer, dimer and hexamer modeled from the crystal structure of aspart insulin (PDB ID 4GBG) using Crysol [24]. The oligomeric distribution of insulin in solution obtained from SAXS measurements was evaluated by using the program Oligomer [25], after computing the form factor for each association state using Crysol [24] and the insulin crystal structure (PDB ID 4GBG.pdb) and their respective oligomers generated by crystallographic symmetry-operations with PyMOL [32].

2.4. Protein crystallography

We crystallized the aspart insulin using hanging-drop vapor-diffusion with drops of equal volume of insulin formulation and crystallization buffer (2 μL) and equilibrating over 500 μL of well solution. Crystals with good diffraction quality were obtained at temperature of 20 °C (Table 1), from crystallization buffers containing 100 mM MES pH 6.5, 1.6 M magnesium sulfate heptahydrate (crystallization buffer 1, pH 6.5; Hampton's Crystal Screening II #20, HCSII20) or 100 mM Tris pH 8.5, 1.5 M ammonium sulfate, 12% v/v glycerol (crystallization buffer 2, pH 8.5; Hampton's Crystal Screening II #42, HCSII42). Crystals of approximately 50 to 100 μm grew over approximately 4 days. Crystals of aspart insulin grown in HCSII20 were soaked in the same buffer supplemented with glycerol 10% v/v to avoid ice formation and ice ring diffraction, just prior to flash freezing. Frozen crystals were subjected to X-ray diffraction and data collection at 100 K under nitrogen stream in the following systems:

i) the MX1 synchrotron beamline [26] from the National Synchrotron Light Laboratory, Campinas, Brazil (LNLS-CNPEM), recorded on a MARCCD165, with wavelength of 1.6080 Å;

Table 1
Summary of crystal diffraction data collection and refinement statistics. Numbers in parentheses denote values in the highest resolution shell.

Parameters/crystal structure ID	4GBN.pdb	4GBC.pdb	4GBI.pdb	4GBK.pdb	4GBL.pdb
pH	6.5	6.5	6.5	8.5	8.5
Beam line	SuperNova's CuKα	SuperNova's CuKα	LNLS-MX1	LNLS-MX2	LNLS-MX2
Detector	Agilent Titan	Agilent Titan	MarCCD 165	MarMosaic225 CCD	MarMosaic225 CCD
Wavelength (Å)	1.54056	1.54056	1.608	1.461	1.461
Space group	R3	R3	R3	R3	R3
Unit cell dimension (Å)	78.710, 37.040	78.150, 36.850	78.290, 36.910	77.500, 37.600	78.570, 37.730
Resolution range (Å)	39.4–1.87 (1.92–1.87)	17.77–1.77 (1.88–1.78)	24.96–2.39 (2.53–2.40)	38.75–2.40 (2.53–2.40)	39.28–2.50 (2.64–2.50)
Monomers/asymmetric unit	2	2	2	2	2
Multiplicity	1.7 (1.2)	1.6 (1.0)	1.7 (1.6)	2.8 (2.7)	2.2 (2.1)
Completeness (%)	97.7 (97.7)	94.8 (82.4)	86.1 (68.1)	96.9 (98.7)	98.3 (97.4)
I/σ	7.8 (2.4)	6.8 (1.0)	5.6 (1.1)	4.2 (1.0)	3.1 (0.9)
Structure refinement					
Rfactor[a] (%)	16.4 (20.4)	16.7 (23.0)	15.2 (13.6)	19.8 (31.5)	19.9 (26.3)
Rfree[b] (%)	21.4 (44.7)	22.3 (23.0)	20.2 (28.3)	26.5 (38.7)	26.1 (28.2)
Number of Reflections in Working Set	6341 (469)	7295 (432)	2370 (179)	3036 (218)	2653 (159)
Number of Reflections in Test Set	334 (15)	370 (19)	232 (17)	138 (7)	242 (21)
B factor (Å^2) Wilson	27.0	32.2	44.6	52.3	53.9
Overall	22.3	28.6	43.6	63.7	66.4
RMSD bond angle (degree)	2.0	1.61	1.95	2.03	1.84
RMSD bond length (Å)	0.020	0.013	0.018	0.018	0.016

[a] *R*-factor = Σhkl|(|Fo| − |Fc|)|/Σ|Fo|, for a working set comprising at least 90% of the data.
[b] *R*-free = Σhkl|(|Fo| − |Fc|)|/Σ|Fo|, for a test set comprising at least 5% of the data selected randomly.

ii) the MX2 synchrotron beamline [27] from the National Synchrotron Light Laboratory, Campinas, Brazil (LNLS-CNPEM), with the diffraction intensities recorded using a MarMosaic 225 detector (MAR Research GmbH, Norderstedt, Germany), with a wavelength of 1.4610 Å;
iii) a home source, using CuKα radiation generated by a NOVA source installed in a SuperNova diffractometer (Agilent) operated at 50 kV and 0.8 mA, and recorded on a Titan (Agilent) area detector.

The images were indexed and processed with either Mosflm [28] or CrysAlisPro [29] and scaled with Scala [30]. The complex was solved by molecular replacement using MolRep [31] or Phaser [32] and PDB entry 1ZEG [13] as a search model, resulting in a clear solution for a dimer in the asymmetric unit. Crystals of aspart insulin were found to have two twin domains, one with a twin operator H, K, L and another with operator K, H, -L and a fraction of approximately 25 to 35%, varying according to the crystal. Diffraction data were detwinned accordingly in Refmac [33]. Real space refinement was conducted by visual inspection of both the map and the model with Coot [34], which was also used to model the water molecules and zinc ions among other cocrystallized molecules. Data quality allowed the proper modeling of the conformation at the region comprising the aminoacids 1–8 of the chain B and the clear identification of the R conformation in one of the monomers and the T conformation in the other one, and thus characterizing the T_3R_3 hexamer. The structure was further refined using Refmac [33]. A summary of crystal parameters along with data collection and refinement statistics are presented in Table 1. Structural validation of the model performed with PROCHECK [35]. A detailed report of the crystallographic statistics can be found in Table 1. All figures were generated with PyMOL [36]. Global pairwise alignment of the insulin structures was performed using ProSMART [37] considering the two monomers in the asymmetric unit as a single structural unit, and achieve the global RMSD corresponding to the superposition of two pairs of monomers. The atomic coordinates have been deposited with the Protein Data Bank and have been assigned the codes depicted in Table 1.

3. Results

3.1. Ion mobility mass spectrometry

In order to gain insight on the oligomeric distribution of aspart insulin in its pharmaceutical formulation we have conducted electrospray ionization–ion mobility spectrometry–mass spectrometry (ESI–IMS–MS) measurements. The combination of electron spray ionization with ion mobility and mass spectrometry allows the separation and accurate measurement of molecular species in a polydisperse system by the decrease in spectral congestion, with the accurate evaluation of their molecular weight, charge and oligomeric states [8,38–42]. Previous work on IMS with aspart insulin suggested that only monomers and hexamers of the aspart insulin would be populated in solution in the presence of zinc and phenol, with no detectable amounts of any other oligomeric species, while monomers, dimers and hexamers are found for the regular insulin [8].

The aspart insulin from its pharmaceutical formulation showed few and well separated distribution of ionic species in the drift and *m/z* space, both when prepared at native-like solution condition (i.e., ammonium acetate buffer pH 7.4) (Fig. 1A, C, E, G, I) and at a denaturing condition (i.e., 1% formic acid) (Fig. 1B, D, F, H, J). Among the major peaks we observed the one corresponding to the monomeric specie of charge 4+, with ~1400 *m/z* and the one corresponding to the monomeric specie of charge +3, with ~1940 *m/z* (Fig. 1A and B). By applying ESI–IMS–MS stripping in the drift space spectra at the 1940 *m/z* region (Fig. 1C and D) we observed the existence of two populations with distinct drift time (Fig. 1E and F). ESI–IMS–MS stripping of the drift-time spectra allowed the deconvolution of the mass spectra, revealing both monomeric, +3 ionic specie (Fig. 1G and H), and dimeric, +6 ionic specie (Fig. 1I and J), both at native-like (Fig. 1G and I) and denaturing (Fig. 1H and J) conditions. Each peak associated with the +3 and the +6 charges for respectively aspart insulin monomer and dimer (Fig. 1E and F) were reasonably narrow, about 1 ms FWHM, and satisfactorily resolved in the drift time axis, allowing the unambiguous identification of these distinctive oligomeric species in solution but with

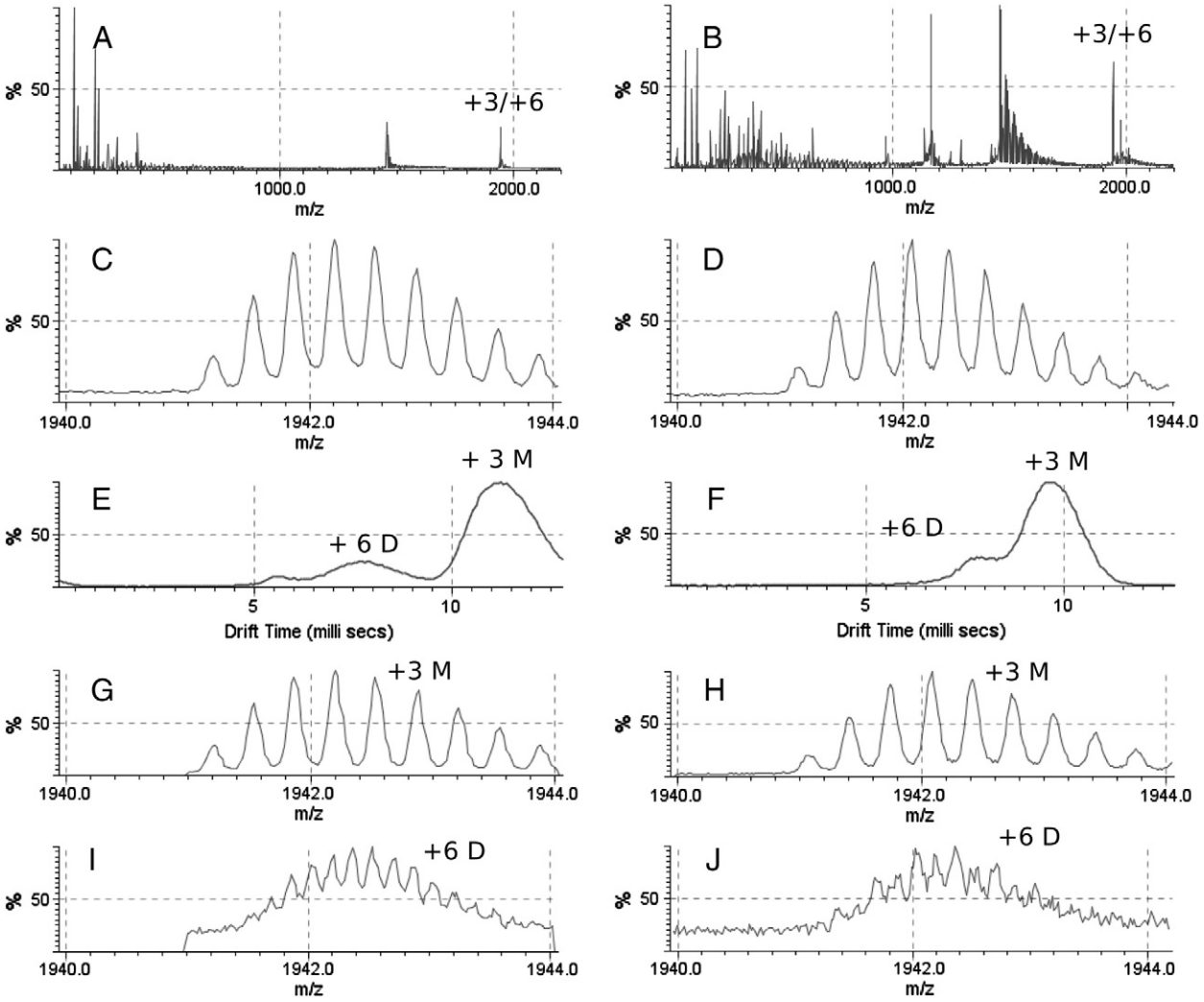

Fig. 1. Ion mobility mass spectrometry assay of aspart insulin. Aspart insulin was diluted 20 times with 100 mM ammonium acetate pH 7.4 (A, C, E, G, I) or 49% methanol in water with 1% formic acid (B, D, F, H, J) and injected at a rate of 100 nL/min and the spectra were accumulated for 5 min at 3 s steps. (A and B) raw mass spectra of aspart insulin at native and denaturing conditions, respectively; (C and D) magnification of the mass range that include the +3 monomer (+3 M; see panel G and H) and the +6 dimer (+6 D; see panels I and J); (E and F) ion mobility spectra for the regions respectively in panels C and D, comprising the +3 monomer and +6 dimer; (G and H) mass spectra of the +3 monomer at native (panel E) and denatured (panel F) conditions; (I and J) mass spectra of the +6 dimer at native (panel E) and denatured (panel F) conditions.

similar *m/z* ration which otherwise would not be possible. Hexamers can also be detected with charged states +11 and +10, revealing the existence of stable hexamers in solution (not shown) and in good agreement with previous report [8]. Collectively, these data suggest that the balance between the conformational states fluctuate between hexamers and monomers through the highly stable dimeric specie.

3.2. Small-angle X-ray scattering analysis of insulin formulation

We measured the small-angle X-ray scattering (SAXS) of two insulin formulations. SAXS has long been used to identify the quaternary organization of proteins, including insulin and insulinomimetic compounds at varying compositions [14,21,22]. The scattering curves of both regular insulin and aspart insulin were superimposable, both at their original concentration (Fig. 2A, B, C) and when diluted (Fig. 2D, E, F). The concentration dependence of the quaternary organization of insulin was probed by measuring the SAXS of the insulin formulation in its original pharmaceutical formulation (100 U/mL; Fig. 2A) and at a diluted concentration (33 U/mL; Fig. 2D). Analysis of the SAXS data revealed that dilution at this concentration range did not affect either insulin scattering profile, and had only minor effect in the overall structural parameters (Table 2). The absence of drift in the linearity of the Guinier analysis revealed the absence of supramolecular aggregates [20] (Fig. 2B, E), suggesting a major oligomeric form in solution and the absence of detectable aggregate in both formulations. A real-space analysis obtained from the Fourier transform of the scattering profile using Gnom [23] allowed the recovery of mean structural parameters of the insulin in their formulations, including the maximum distance (Dmax of approximately 48 Å) and the radii of gyration (R_g of approximately 19 Å), which were equivalent within error for both aspart and regular insulin variants (Table 2) The obtained pair-distribution function $P(r)$ also revealed a similar molecular shape for all formulations, at their original concentration (Fig. 2C) and the diluted concentration (Fig. 2D), ruling out any major concentration-dependent effect under the present analytical conditions. Together, these data indicate the similarity in high-order quaternary distribution between aspart and regular insulin, suggesting that the two insulin variants show close oligomeric distribution in solution.

Adjusting the experimental data with crystallographic structural models assuming only monomeric or dimeric insulin in solution resulted in high discrepancy values (χ^2) of 5 or above, suggesting a lack of compatibility with the oligomeric distribution of insulin in the measured samples (Fig. 3; Table 2). Fitting the scattering data using hexameric insulin provided lower discrepancy values of about 1.5,

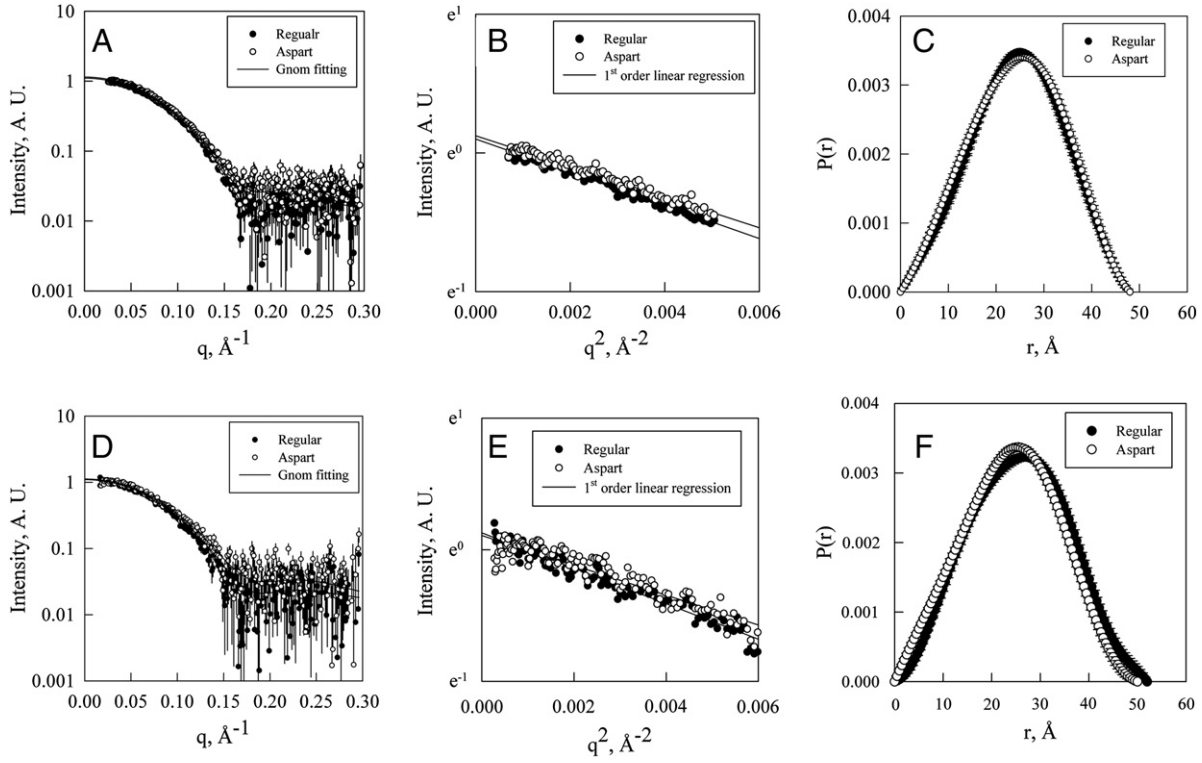

Fig. 2. Small-angle X-ray scattering (SAXS) analysis of aspart insulin. Scattering profiles of insulin variants: aspart (●) and regular (○). SAXS measurements were performed at 100 U/mL (A, B, C) and 33 U/mL (diluted with type-I water immediately prior to measurements, D, E, F). A and D, $I(q)$ scattering curves. Lines correspond to best adjustments with Gnom. B and E, Guinier plot. The linearity of the Guinier plot indicates that insulin solutions are monodispersed. C and F, pair-distance distribution for insulin formulations. Details are in Materials and methods section and in Table 2.

although visual inspection of the experimental data reveals a lack of tight correspondence between the experimental SAXS data and the theoretical fitting (Fig. 3). The experimental scattering data could be better fitted by using a set of oligomers models (monomer, dimer and hexamer), allowing the description of an ensemble of varying oligomeric species in equilibrium in solution. The volume fraction of each individual species in the sample was then computed, reaching a scattering function which best adjust to the experimental solution scattering data, with low discrepancy between theoretical fitting and the scattering data, both for the regular (Fig. 3A) and the aspart (Fig. 3B) insulin. For regular insulin the best fitting was achieved assuming a composition of 64% hexamers and 36% dimers (Fig. 3A), while the aspart insulin was better described with a distribution comprising 55% hexamers, 25% dimers and 20% monomers (Fig. 3B). Together, these data suggest that insulin might populate an equilibrium distribution of the above mentioned volume fraction of hexamers, dimers and monomers at the concentration and composition evaluated here, i.e., their original pharmaceutical formulation.

Table 2
Small-angle X-ray scattering analysis of aspart and regular insulin.

	Regular	Aspart
Diluted (33 U/mL)		
R_g, Å		
Guinier	18.9 ($r^2=0.927$)	18.4 ($r^2=0.865$)
P(r)	18.8 ± 0.08	18.4 ± 0.08
Dmax, Å	50 ± 2	50 ± 2
Concentrated (100 U/mL)		
R_g, Å		
Guinier	18.7 ($r^2=0.971$)	18.2 ($r^2=0.958$)
$P(r)$	18.6 ± 0.03	18.6 ± 0.04
D_{max}, Å	48 ± 1	48 ± 2
Fitting analysis[a]		
Discrepancy value χ^2		
Monomer	13.5	11.0
Dimer	6.8	5.2
Hexamer	1.5	2.0
Distribution (M + D + H)	1.5	1.4
Volume fraction		
Monomer	0.00 + 0.00	0.20 + 0.06
Dimer	0.36 + 0.01	0.25 + 0.05
Hexamer	0.64 + 0.01	0.55 + 0.01

[a] Calculated using Crysol [24] and Oligomer [25] and insulin crystal structure (PDB ID 4GBG.pdb) and oligomers generated by crystallographic symmetry-operations with PyMOL [36].

3.3. Crystallographic analysis of the human insulin aspart analog

We have crystallized the human insulin aspart analog by using vapor diffusion technique. A large sparse-matrix screen was performed with sparse-matrix, and the best hits were obtained using as precipitant: i) 100 mM MES pH 6.5, 1.6 M magnesium sulfate heptahydrate and ii) 100 mM Tris pH 8.5, 1.5 M ammonium sulfate, 12% v/v glycerol. Both crystallization conditions allowed us to obtain insulin aspart crystals within a few days with good diffraction quality. Aspart insulin crystals grown at both pH 6.5 and pH 8.5 belong to the R3 space group and have similar cell parameters (Table 1).

The crystal structures of aspart insulin at pH 6.5 and at pH 8.5 reported here were solved by molecular replacement, with a dimer in the asymmetric unit (Fig. 4). The region comprising aminoacids 1 to 8 is involved in the "T" conformation in one monomer and in the "R" conformation in the other monomer, and both could be well modeled in electron density (Fig. 4A). Two zinc ions are located approximately 16 Å apart on this channel, each one forming a typical tetrahedral coordination sphere involving three imidazolic nitrogens of B10His (one histidine from each dimer; not shown). In all the aspart insulin structures reported here, three symmetry-related "TR" dimers form

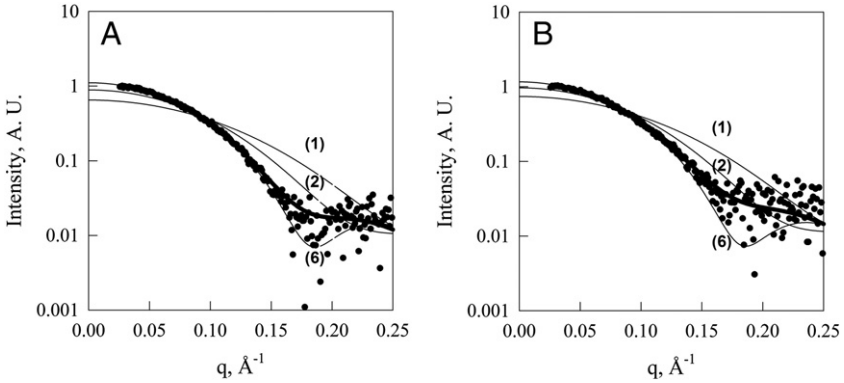

Fig. 3. Evaluation of oligomeric distribution of insulin in solution. The scattering profiles (dots) of the insulin variants regular (A) and aspart (B) at 100 U/mL were fitted with monomeric (1), dimeric (2) and hexameric (6) structural models of insulin derived from crystallographic data (PDB ID 4GBG). A fitting was performed considering a mixed composition of monomers, dimers and hexamers (tick line), resulting in the best fitting. Details are in the Materials and methods section and in Table 2.

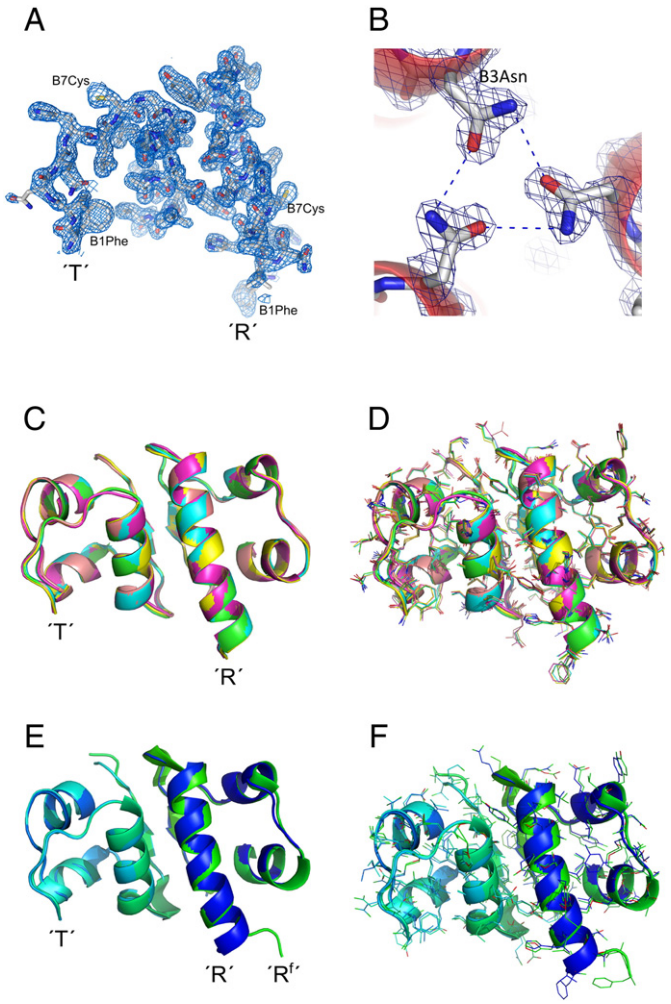

Fig. 4. Crystallographic analysis of aspart insulin. "T," "R" and "Rf" are shown in the figure close to the B1Phe of the monomer in the respective conformation. (A) Details of |2Fo − Fc| electron density map contoured at 1 σ of the B1–16 segment in both the "T" and "R" conformers of the aspart insulin (PDB entry 4GBC). Images were generated with PyMOL [36]. (B) Details of |2Fo − Fc| electron density map contoured at 1 σ of the three B3Asn from the "R" conformers of the hexameric T_3R_3 aspart insulin (PDB entry 4GBC). (C) Ribbon and (D) ribbon with side-chain representation of the superposition of the 5 present T_3R_3 aspart insulin crystal structures. (E) Ribbon and (F) ribbon with side-chain representation of the superposition of the T_3R_3 crystal structures of the present aspart insulin (PDB entry 4GBC; blue) and the $T_3R^f_3$ conformer of the regular human insulin ($T_3R^f_3$; PDB entry 1TRZ).

the insulin hexamer, arranged around a crystallographic 3-fold axis, collinear with the central channel. The aminoacid Asn3 from the chain B face toward the interior of the channel, performing a stable electrostatic interaction with the two symmetry-related B3Asn (Fig. 4B). This orientation is also seen in other insulin structures, but not so close or even demanding water molecules as a coordinating molecule for B3Asn.

All five aspart insulin crystal structures reported here superpose with high similarity for both Cα (Fig. 4C) and side chains (Fig. 4D), showing only minor positional variations of aspart insulin side chains. Superposition of the present aspart insulin with wild-type human insulin at conformation $T_3R^f_3$ (PDB entry 1TRZ) evidences the dissimilarity in the aminoacids 1 to 3 from chain B, both for backbone (Fig. 4E) and side-chains (Fig. 4F), corroborating the aspart insulin in the T_3R_3 conformation with a pure R-state conformation. A pairwise global structural alignment of the present T_3R_3 aspart insulin structures reveals highlights their similarity (Table 3), with global RMSD of less than 0.5 Å, regardless of the tested variables on the crystallization and data collection of the aspart insulin.

4. Discussion

We showed here that a T_3R_3 conformer can be achieved for the hexameric aspart insulin. These data indicate the conformational plasticity of the aspart insulin even at hexameric assembly, being able to convert from a full-R (R_6) conformer to a structure with the T state (T_3R_3).

In the present SAXS measurements, we inferred similar mean oligomeric organization for both aspart and regular human insulin, with equivalent scattering profiles (Fig. 2) and structural parameters (Table 2). Both the present work and previous work [13] show the ability of aspart insulin to associate into hexamers, despite its enhanced propensity for dissociation into monomers compared to regular insulin [12], prompting faster absorption [15].

Table 3
Pairwise global structural alignment of the aspart insulin crystal structures. The insulin structures were superposed by pairwise global alignment using ProSMART [37] and the RMSD was calculated and is reported here.

Global pairwise structural alignment		pH 6.5			pH 8.5	
		4GBN.pdb	4GBC.pdb	4GBI.pdb	4GBK.pdb	4GBL.pdb
pH 6.5	4GBN.pdb	–	0.29	0.39	0.47	0.36
	4GBC.pdb	–	–	0.42	0.37	0.42
	4GBI.pdb	–	–	–	0.47	0.41
pH 8.5	4GBK.pdb	–	–	–	–	0.45
	4GBL.pdb	–	–	–	–	–

In a previous work using ESI–IMS–MS the dimeric species was not detected for the aspart insulin, only for the regular insulin, suggesting that dimers could only exist for the more stable, wild-type form of insulin. Instead, the present ESI–IMS–MS data reported here allowed the clear separation and identification of a high level of the dimeric species, co-populated with the same m/z (approximately 1942 m/z) of the monomeric specie but with dissimilar charges ($+6$ and $+3$, respectively). The use of ESI–IMS–MS allowed the identification of the aspart insulin with a satisfactory sensitivity for its oligomeric distribution, which in addition to previous results [38] evidences that the balance between these species is under tightly influence of the composition of the formulation, and minor variations on its might exert considerable changes on the polymorphic distribution of protein conformation and assembly. These data add further evidences that the ESI–IMS–MS would assist in obtaining a fingerprint signature of protein products.

Collectively, the present work introduces a new perspective on the conformational plasticity of the aspart insulin variant, introducing new avenues in the understanding of the conformational variability in the hexameric assembly.

Acknowledgments

We would like to thank MS Marcela Rosa (INMETRO) for helpful assistance and Dr. Gustavo H. M. F. de Souza (Research Scientist, HRMS Bio Applications, Waters Corporation — Brazil) for helpful discussion on ESI–IMS–MS data analysis. This research was supported by the CAPES, CNPq, INCT-CNPq, FAPERJ, LNLS and Instituto Nacional de Metrologia, Normalização e Qualidade Industrial (INMETRO). Funding agencies had no role in study design, data collection or analysis.

References

[1] T.L. Blundell, J.F. Cutfield, S.M. Cutfield, E.J. Dodson, G.G. Dodson, D.C. Hodgkin, D.A. Mercola, M. Vijayan, Nature 231 (1971) 506–511.
[2] H.B. Olsen, S. Ludvigsen, N.C. Kaarsholm, Biochemistry 35 (1996) 8836–8845.
[3] P.S. Brzovic, W.E. Choi, D. Borchardt, N.C. Kaarsholm, M.F. Dunn, Biochemistry 33 (1994) 13057–13069.
[4] A.D. Kline, R.M. Justice Jr., Biochemistry 29 (1990) 2906–2913.
[5] Q. Hua, M.A. Weiss, Biochemistry 30 (1991) 5505–5515.
[6] W. Kadima, M. Roy, R.W. Lee, N.C. Kaarsholm, M.F. Dunn, Journal of Biological Chemistry 267 (1992) 8963–8970.
[7] X. Chang, A.M. Jorgensen, P. Bardrum, J.J. Led, Biochemistry 36 (1997) 9409–9422.
[8] R. Salbo, M.F. Bush, H. Naver, I. Campuzano, C.V. Robinson, I. Pettersson, T.J. Jorgensen, K.F. Haselmann, Rapid Communications in Mass Spectrometry 26 (2012) 1181–1193.
[9] M. Adams, T. Blundell, E. Dodson, G. Dodson, M. Vijayan, E. Baker, M. Harding, D. Hodgkin, B. Rimmer, S. Sheat, Structure of Rhombohedral 2 Zinc Insulin Crystals, 1969, pp. 491–495.
[10] E. Ciszak, G.D. Smith, Biochemistry 33 (1994) 1512–1517.
[11] R. Sreekanth, V. Pattabhi, S.S. Rajan, Biochimie 90 (2008) 467–473.
[12] J. Brange, U. Ribel, J.F. Hansen, G. Dodson, M.T. Hansen, S. Havelund, S.G. Melberg, F. Norris, K. Norris, L. Snel, A.R. Sørensen, H.O. Voigt, Nature 333 (1988) 679–682.
[13] J.L. Whittingham, D.J. Edwards, A.A. Antson, J.M. Clarkson, G.G. Dodson, Biochemistry 37 (1998) 11516–11523.
[14] V.N. Uversky, L.N. Garriques, I.S. Millett, S. Frokjaer, J. Brange, S. Doniach, A.L. Fink, Journal of Pharmaceutical Sciences 92 (2003) 847–858.
[15] P.D. Home, L. Barriocanal, A. Lindholm, European Journal of Clinical Pharmacology 55 (1999) 199–203.
[16] R.H. Becker, Diabetes Technology & Therapeutics 9 (2007) 109–121.
[17] A. Wagner, J. Diez, C. Schulze-Briese, G. Schluckebier, Proteins 74 (2009) 1018–1027.
[18] J.P. Williams, J.A. Lough, I. Campuzano, K. Richardson, P.J. Sadler, Rapid Communications in Mass Spectrometry 23 (2009) 3563–3569.
[19] G. Kellermann, F. Vicentin, E. Tamura, M. Rocha, H. Tolentino, A. Barbosa, A. Craievich, I. Torriani, Journal of Applied Crystallography 30 (1997) 880–883.
[20] A. Guinier, G. Fournet, Small-angle Scattering of X-rays, John Wiley & Sons, NY, 1955.
[21] L. Nielsen, S. Frokjaer, J. Brange, V.N. Uversky, A.L. Fink, Biochemistry 40 (2001) 8397–8409.
[22] L.M. Lima, C.F. Becker, G.M. Giesel, A.F. Marques, M.T. Cargnelutti, N.M. de Oliveira, R.Q. Monteiro, H. Verli, I. Polikarpov, Biochimica et Biophysica Acta 1794 (2009) 873–881.
[23] D.I. Svergun, Journal of Applied Crystallography 25 (1992) 495–503.
[24] D. Svergun, C. Barberato, M.H.J. Koch, Journal of Applied Crystallography 28 (1995) 768–773.
[25] P.V. Konarev, V.V. Volkov, A.V. Sokolova, M.H.J. Koch, D.I. Svergun, Journal of Applied Crystallography 36 (2003) 1277–1282.
[26] I. Polikarpov, L.A. Perles, R.T. de Oliveira, G. Oliva, E.E. Castellano, R.C. Garratt, A. Craievich, Journal of Synchrotron Radiation 5 (1998) 72–76.
[27] B.G. Guimaraes, L. Sanfelici, R.T. Neuenschwander, F. Rodrigues, W.C. Grizolli, M.A. Raulik, J.R. Piton, B.C. Meyer, A.S. Nascimento, I. Polikarpov, Journal of Synchrotron Radiation 16 (2009) 69–75.
[28] A.G. Leslie, Joint CCP4 + ESF-EAMCB Newsletter on Protein Crystallography, 1992.
[29] Agilent Technologies, CrysAlisPro Software system, Agilent Technologies UK Ltd., Oxford, UK, 2011.
[30] N.4. Collaborative Computational Project, Acta Crystallographica (1994) 760–763.
[31] A. Vagin, A. Teplyakov, Journal of Applied Crystallography 30 (1997) 1022–1025.
[32] A.J. McCoy, R.W. Grosse-Kunstleve, P.D. Adams, M.D. Winn, L.C. Storoni, R.J. Read, Journal of Applied Crystallography 40 (2007) 658–674.
[33] G.N. Murshudov, A.A. Vagin, E.J. Dodson, Acta Crystallographica Section D: Biological Crystallography 53 (1997) 240–255.
[34] P. Emsley, K. Cowtan, Acta Crystallographica Section D: Biological Crystallography 60 (2004) 2126–2132.
[35] R.A. Laskowski, J.A.C. Rullmann, M.W. MacArthur, R. Kaptein, J.M. Thornton, Journal of Biomolecular NMR 8 (1996) 477–486.
[36] W.L. DeLano, The PyMOL Molecular Graphics System, DeLano Scientific LLC, San Carlos, CA, USA, 2002.
[37] R. Nicholls, PhD R. Nicholls, University of York, 2011.
[38] S.A. Berkowitz, J.R. Engen, J.R. Mazzeo, G.B. Jones, Nature Reviews. Drug Discovery 11 (2012) 527–540.
[39] I.A. Kaltashov, C.E. Bobst, R.R. Abzalimov, S.A. Berkowitz, D. Houde, Journal of the American Society for Mass Spectrometry 21 (2010) 323–337.
[40] D.P. Smith, T.W. Knapman, I. Campuzano, R.W. Malham, J.T. Berryman, S.E. Radford, A.E. Ashcroft, European Journal of Mass Spectrometry 15 (2009) 113–130, (Chichester, Eng).
[41] D.P. Smith, S.E. Radford, A.E. Ashcroft, Proceedings of the National Academy of Sciences of the United States of America 107 (2010) 6794–6798.
[42] B.T. Ruotolo, K. Giles, I. Campuzano, A.M. Sandercock, R.H. Bateman, C.V. Robinson, Science 310 (2005) 1658–1661.